Non-sacrificial additive regulated electrode-electrolyte interface enables long-life, deeply rechargeable aqueous Zn anodes

Ang Li[a], Xinyu Zhang[a], Zeyu Xu[a], Maochun Wu[a,*]

[a] *Department of Mechanical Engineering, The Hong Kong Polytechnic University, Hong Kong SAR, 999077, PR China*

* Corresponding author.

E-mail address: maochun.wu@polyu.edu.hk (M.C. Wu).

Abstract

Rechargeable aqueous Zn batteries (RAZBs) offer a promising solution for safe and cost-effective energy storage. However, practical applications of this type of battery are hindered by dendrite formation and side reactions, which primarily stem from the unstable Zn electrode-electrolyte interface (EEI). Here, we report 3-(1-pyridinio)-1-propanesulfonate (PPS) as a novel EEI regulator to tackle these critical issues. Theoretical calculations and experimental results reveal that PPS molecules can be preferentially adsorbed on the Zn anode surface and construct a lean-water EEI, which regulates uniform Zn plating/stripping and minimizes interfacial side reactions. As a result, the addition of PPS enables a Zn//Cu asymmetric cell to achieve an ultra-high Coulombic efficiency of 99.88% and a lifespan of over 4,000 cycles (around half a year), far exceeding that with a conventional electrolyte (99.65% and 210 cycles). Remarkably, even at 20 mA cm^{-2} and a high depth of discharge of 70%, the Zn//Zn battery using the new electrolyte can still maintain an impressive cycling life of over 250 h. More importantly, the implementation of the designed electrolyte in various Zn-

based full cells yields exceptional capacity retention and lifespan. This work underscores the importance of EEI regulation in advancing RAZB technology and offers a simple yet effective strategy for enhancing the stability and reversibility of Zn anodes, which represents a key step toward realizing the full potential of RAZBs for next-generation energy storage.

Keywords: Rechargeable aqueous Zn batteries; Zn anode; electrode-electrolyte interface; electrolyte additive; 3-(1-pyridinio)-1-propanesulfonate.

1. Introduction

The grave concerns over energy crisis and environmental problems have sparked great interest in the deployment of renewable energy such as wind and solar power, which necessitates large-scale energy storage technologies to smooth out their intermittency [1-5]. Rechargeable batteries represent one of the most promising electrochemical energy storage devices due to their attractive features such as high efficiency, site-independency, high design flexibility, and good scalability [6-9]. Particularly, Li-ion batteries have dominated the electrochemical energy storage market, with a wide range of applications ranging from consumer electronics to electric vehicles [10-13]. However, their market penetration into grid storage is hindered by the high cost and serious safety concerns [14-16]. In contrast, rechargeable aqueous Zn batteries (RAZBs) provide a safe and low-cost alternative for this application due to their unique characteristics [17-19]. First, RAZBs use earth-abundant Zn metal as anode, which also has a high specific capacity and a suitable redox potential [20-22]. Meanwhile, the use of water-based electrolytes not only eliminates the safety issues but also offers high rate

capability thanks to the higher ionic conductivities [23, 24]. These remarkable features make RAZBs one of the most promising technologies for large-scale energy storage [25-27].

Unfortunately, RAZBs suffer from low Coulombic efficiencies (CEs) and short cycle life, primarily due to the formation of Zn dendrites and side reactions [5, 11, 28, 29]. Up to now, a wide variety of strategies, including construction of artificial interphase [30-32], modification of separators [33-35], introduction of electrolyte additives [7, 25, 36-45], and so on, have been attempted to overcome the two intertwined challenges. Among these, employing electrolyte additives has attracted the most attention for its simplicity, efficiency, and scalability [46]. For instance, various organic solvents, such as *N*-methyl-2-pyrrolidone (NMP) [47], dimethyl sulfoxide [48], and *N*, *N*-dimethylacetamide [49], have been added into the electrolyte. In the organic-molecule-modulated electrolytes, the solvation structure of Zn^{2+} may be reconfigured and the hydrogen bonding network among water molecules may be interrupted, leading to uniform Zn deposition and suppressed side reactions. However, this strategy often involves large amounts of organic solvents, casting a shadow on the inherent non-toxic, low-cost, and eco-friendly features of aqueous electrolytes. In addition, the use of organic cosolvent may result in a significant decrease in ionic conductivity of the electrolyte, thus imposing a penalty on the rate capability and practical energy density of full batteries [6]. It is worth noting that Zn plating/stripping and side reactions occur mainly at the Zn electrode-electrolyte interface (EEI), whose thickness is at an angstrom level [50]. Therefore, regulating the EEI that determines the electrochemical

performance of Zn anodes by taking advantage of additives represents a more promising option. To this end, Wu *et al.* proposed an electrolyte containing trifluoroacetamide, which was decomposed to form a ZnF_2-rich solid electrolyte interphase (SEI) on the anode surface [51]. Similarly, Wang and co-workers prepared a 2,3,4,5-tetrahydrothiophene-1,1-dioxide-added electrolyte [52], which led to the formation of organic-inorganic composite SEI. These *in-situ* produced SEI layers can block water molecules and modulate Zn^{2+} fluxes, thus prolonging the lifespan of RAZBs. However, the durability of these SEI layers remains a concern, particularly under long-term and/or deep charge-discharge conditions as the continuous degradation and regeneration of the SEI layer will progressively deplete additives and eventually lead to battery failure. Therefore, there is an urgent need to develop a stable and highly efficient electrolyte additive as an EEI modulator to overcome rampant dendrites and side reactions, thereby realizing highly stable and reversible Zn anodes. To effectively regulate the EEI, the additive molecules should first contain polar groups to ensure preferential adsorption on Zn surface under electrostatic or electric fields. Moreover, structural stability is also necessary for the additives to dynamically regulate the interfacial environment and thus enable high anode reversibility during long-term and deep charging and discharging. Additionally, the additive should have certain solubility in the aqueous electrolytes.

Herein, 3-(1-pyridinio)-1-propanesulfonate (PPS, chemical formula shown in Fig. S1) is introduced into conventional $ZnSO_4$ electrolyte for its unique structural features to effectively reshape the EEI environment with minimal effect on the bulk electrolyte.

The sulfonic acid group of PPS has strong polarity and good affinity with Zn metal [50, 53], while the positively charged *N*-alkylpyridinium group not only makes the molecule electrically neutral but can be strongly adsorbed on the Zn surface under the action of the electric field during electroplating, which serves as the basis for the preferential adsorption [54, 55]. Furthermore, the electropositive *N*-alkylpyridinium group and the electronegative sulfonic acid group are separated by three carbon atoms, making PPS less susceptible to reduction [7]. This appropriate carbon chain length also achieves a trade-off between additive solubility and localized hydrophobicity. Consequently, PPS molecules can be preferentially adsorbed on the Zn surface, which not only regulates the uniform diffusion and deposition of Zn^{2+}, ensuring a dense and flat electrode surface during electroplating, but also creates a water-deficient EEI that considerably alleviates side reactions. As a result of the finely tuned EEI, the cycle life of Zn//Zn symmetric battery is dramatically extended from 120 to 3,000 h at 2 mA cm^{-2} and 1 mA h cm^{-2}. Moreover, the Zn//Zn symmetric battery with the newly designed electrolyte can be cycled for more than 250 h under harsh conditions of 20 mA cm^{-2} with 70% depth of discharge (DoD). More remarkably, when the PPS-modulated electrolyte is applied to full cells, a Zn//$Cu_xV_2O_5 \cdot nH_2O$ cell displays excellent capacity retention of 87.50% after 3,000 cycles at 5 A g^{-1} and a Zn//activated carbon (AC) hybrid supercapacitor operates stably for 65,000 cycles. These results highlight the effectiveness of PPS in addressing the key challenges facing Zn anodes.

2. Results and discussion

2.1 Determination of optimal PPS concentration

First, the optimal concentration of PPS was determined by cycling Zn//Zn symmetric cells at 10 mA cm^{-2} with an areal capacity of 10 mA h cm^{-2} using various electrolytes, *i.e.*, pure 2 M $ZnSO_4$ electrolyte (denoted as ZSO) and 2 M $ZnSO_4$ electrolytes containing different concentrations (1, 5, and 10 mM) of PPS (denoted as ZSO+1PPS, ZSO+5PPS, and ZSO+10PPS, respectively). As shown in Figs. 1a and S2, the Zn//Zn symmetric battery assembled with ZSO quickly short-circuits and fails after less than 50 h. By contrast, the cycle life of the battery is extended two-fold in the presence of 1 mM PPS, which is further prolonged to 400 h when the concentration is increased to 5 mM. However, excessive PPS (10 mM) additive adversely affects the cycling stability of the battery, resulting in degradation of battery life compared with 5 mM PPS. Electrochemical impedance spectroscopy (EIS) was then conducted to gain deeper insights into the effect of varying PPS concentrations on the durability of Zn anodes. As displayed in Fig. S3**,** the diameter of the semicircle in the Nyquist plot continuously increases with PPS concentration, suggesting the progressive increase of charge transfer resistance (R_{ct}). This is understandable because PPS will be preferentially adsorbed on the electrode surface, which may slow down the Zn deposition kinetics. The ionic conductivity was found to decrease with increasing PPS concentration (Fig. S4). These results are consistent with the polarizations of Zn//Zn symmetric batteries in Fig. 1a. It can be inferred that excessive additives in the ZSO+10PPS electrolyte hamper Zn^{2+} transfer and deposition kinetics [56], which may trigger Zn dendrite formation and hence lead to premature battery failure. Moreover, Fig. S5 shows that an excess of PPS (10 mM) additive also reduces the pH value of

electrolyte, which will exacerbate hydrogen evolution reaction (HER) that is deleterious to the reversibility and stability of Zn anodes [57]. Conversely, insufficient PPS (in ZSO+1PPS electrolyte) fails to effectively regulate the EEI, which leads to poor side reaction inhibition and Zn deposition regulation. Hence, ZSO+5PPS is selected as the optimized electrolyte for following study.

2.2 Physicochemical properties of electrolytes

Physicochemical properties of various electrolytes were probed by experiments and theoretical calculations to reveal the underlying mechanisms of PPS additive in enhancing the stability and reversibility of Zn anodes. Linear sweep voltammetry (LSV) tests in Fig. S6 show that no additional anodic or cathodic peak appears after PPS is introduced, which indicates that PPS is a non-sacrificial additive capable of continuously regulating the EEI and thus ensures the long-term stability of Zn anodes [58]. This feature is further validated by the X-ray photoelectron spectroscopy (XPS) tests of Zn foils with different etching depths after 20 cycles at 10 mA cm^{-2} with an areal capacity of 10 mA h cm^{-2}. As shown in Fig. S7, no decomposition products of the PPS additive were detected by XPS, confirming the stability of the PPS additive [59-61]. Fourier transform infrared (FT-IR) spectroscopy (Fig. 1b) reveals those peaks corresponding to the stretching vibration of the O−H group (~3365 and ~3223 cm^{-1}), the bending vibration of O−H (~1640 cm^{-1}), and the vibration of SO_4^{2-} (~1084 cm^{-1}) do not alter in position after adding 5 mM PPS. These results indicate that 5 mM PPS does not impact the solvation structure of Zn^{2+} in the bulk electrolyte. Furthermore, nuclear magnetic resonance (NMR) spectra shown in Fig. 1c suggest that ^1H peaks from

155 water in ZSO and ZSO+5PPS electrolytes are consistent in terms of chemical shifts.
156 These results confirm that 5 mM PPS has almost no effect on the hydrogen bonding
157 network of water molecules, which is not surprising as only a small amount of PPS is
158 added into the electrolyte. Therefore, it can also be preliminarily inferred that the main
159 function of PPS additive is the EEI regulation rather than hydrogen bond formation
160 with water or reconfiguration of Zn^{2+} solvation structures in the bulk electrolyte.

161 To prove this hypothesis, density functional theory calculations were performed to
162 study the interaction of PPS and water with three principal crystal planes of Zn metal
163 anode. As presented in Fig. 1d, the PPS molecule exhibits remarkably more negative
164 adsorption energies compared to those of the water molecule, irrespective of the crystal
165 plane orientation. It indicates the preferential adsorption of PPS onto the Zn surface,
166 replacing water molecules and thus creating a water-poor EEI that alleviates water-
167 induced side reactions [62]. Moreover, the energy levels of the lowest unoccupied
168 molecular orbital (LUMO) and the highest occupied molecular orbital (HOMO) of both
169 water and PPS were calculated and compared in Fig. 1e. It is noteworthy that PPS
170 possesses a lower energy of LUMO (−2.03 eV vs. 2.41 eV) and a higher energy of
171 HOMO (−6.56 eV vs. −8.10 eV) compared to H_2O, suggesting stronger electron
172 transfer propensity between PPS and Zn metal, and thus a higher tendency of PPS
173 adsorption onto the anode surface. In addition, the charge density difference of PPS
174 with different crystal planes of Zn shown in Fig. S9 indicates that there are electron
175 cloud overlap and transition inclination between Zn atoms and sulfonic acid groups in
176 PPS molecules, demonstrating that the strong preferential adsorption is primarily driven

177 by the interaction between sulfonic acid group and Zn metal. The preferential
178 adsorption behavior of PPS is further verified by the reduction in differential
179 capacitance (Fig. S10) with the introduction of additives, attributing to the large steric
180 effects of PPS molecules accumulating at the interface [63]. In addition, contact angle
181 measurement was carried out to assess the wettability of ZSO and ZSO+5PPS
182 electrolytes on Zn electrodes. Compared to the large contact angle of 87.71° in ZSO
183 electrolyte, Zn metal foil exhibits a smaller contact angle of 81.93° to ZSO+5PPS
184 electrolyte (Fig. S11). The improved wettability achieved by PPS-added electrolyte is
185 conducive to reducing the interfacial tension and Gibbs free energy of the EEI [64].
186 Based on the classical nucleation theory, ZSO+5PPS electrolyte can bring about a
187 reduced critical nucleation radius during the electrodeposition of Zn^{2+}, thereby
188 resulting in smooth Zn deposition [65].
189

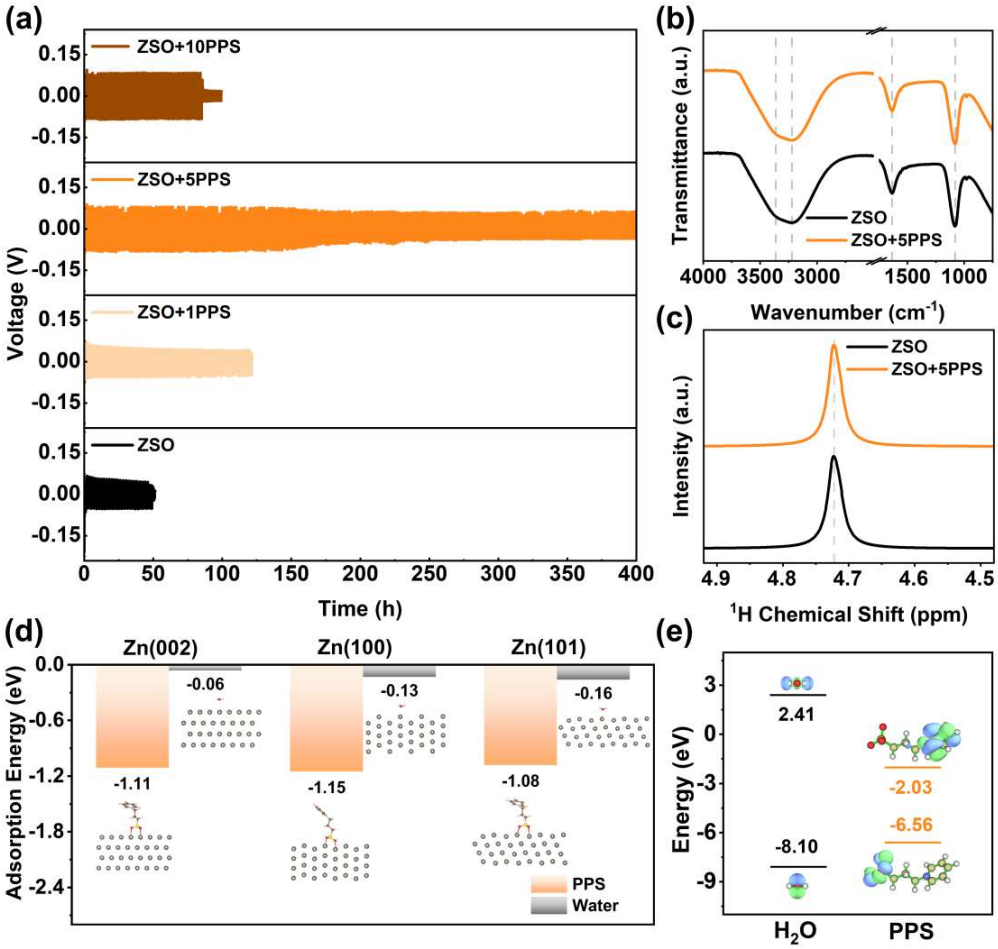

Fig. 1. (a) Long-term galvanostatic charge and discharge (GCD) tests of Zn//Zn symmetric batteries using ZSO and ZSO+5PPS electrolytes at 10 mA cm^{-2} with an areal capacity of 10 mA h cm^{-2}; (b) FT-IR spectra of ZSO and ZSO+5PPS electrolytes; (c) ^{1}H NMR spectra of ZSO and ZSO+5PPS electrolytes; (d) adsorption energy of PPS and water on different crystal planes of Zn anode; and (e) frontier molecular orbital energy of water and PPS.

2.3 Study on Zn deposition behavior modulated by PPS additives

To elucidate the influence of PPS-modulated EEI on Zn electrodeposition, a

homemade *in-situ* optical microscope (OM) observation system was devised to monitor the real-time morphology evolution of Zn during the plating process. As shown in Fig. 2a, Zn electrode surface becomes rough and uneven when subjected to Zn plating in ZSO electrolyte at 10 mA cm^{-2}. By comparison, the Zn electrodeposits are smooth and dense in ZSO+5PPS electrolyte (Fig. 2b), indicating the effective suppression of Zn dendrites by adding PPS additive. To unravel the underlying mechanisms, a series of electrochemical measurements were performed. Cyclic voltammetry (CV) curves in Fig. 2c show that the initial deposition potential of Zn^{2+} in ZSO+5PPS electrolyte negatively shifts compared to blank ZSO electrolyte, implying a larger Zn^{2+} deposition barrier needs to be overcome to initiate Zn nucleation [65]. Moreover, the voltage-time profiles of Zn deposition in Zn//Cu asymmetric cells at 5 mA cm^{-2} and 5 mA h cm^{-2} (Fig. 2d) reveal that the nucleation overpotential is increased from 68 to 86 mV after the addition of 5 mM PPS. According to the classical nucleation theory, a higher nucleation overpotential can decrease the critical nucleation radius, thereby improving the nucleus density [66]. This phenomenon is conducive to the formation of finer and denser Zn nuclei during electroplating and thus dendrite-free Zn deposition. The diffusion and deposition behaviors of Zn^{2+} on the electrode surface during plating were further studied by chronoamperometry (CA) tests using Zn//Zn symmetric batteries. As depicted in Fig. 2e, after applying a voltage of −150 mV, the current response shows a continuous growth trend in blank ZSO electrolyte during the whole electrodeposition process. This trend suggests that the Zn^{2+} undergoes 2D diffusion along the electrode surface and accumulates at the nuclei for deposition as shown in Fig. S13a,

consequently leading to the formation of dendritic Zn deposition with increasing surface area [67]. By contrast, in the presence of PPS, the current maintains constant after a short-term increase in the initial stage, indicating the 3D diffusion pattern of Zn^{2+} vertical to the anode and smooth Zn deposition with nearly constant electrode surface area (Fig. S13b). To prove the effectiveness of PPS in achieving uniform Zn plating and stripping, the morphology of Zn foils after 20 cycles at 10 mA cm^{-2} and 10 mA h cm^{-2} in different electrolytes was observed using OM and scanning electron microscopy (SEM). As can be seen from Fig. S14a and b, the Zn electrode cycled in ZSO electrolyte exhibits a random, irregular, and uneven morphology, while it remains dense, uniform, and smooth after cycling in the PPS-added electrolyte (Fig. S14c and d). SEM images further confirm the formation of dendritic Zn in ZSO electrolytes (Fig. 2f), whereas the Zn anode retrieved from the battery with the designed electrolyte remains relatively flatter (Fig. 2g). It should be noted that post-cycling Zn electrodes in ZSO electrolytes were interspersed with glass fiber separators, posing a risk of causing short circuits. On the contrary, in the PPS-added electrolyte, only a slight voids and pits appear in Zn foil when the separator is removed, which can be attributed to the parts of the Zn surface suffer from impeded deposition due to depletion and insufficient replenishment of Zn^{2+} during plating as the separator is compressed on the Zn electrodes [7]. A 3D laser scanning microscope was also employed to evaluate the surface roughness of Zn. As illustrated in Fig. S15a and c, the Zn foil cycling in the blank electrolyte features a high average roughness (R_a) of up to 52.5 μm, implying the uneven Zn deposition. In contrast, Fig. S15b and d show that the PPS-added electrolyte allows the Zn foil to maintain a

smooth profile with low roughness (R_a = 5.0 μm) after cycling, confirming the effectiveness of PPS in suppressing dendrite growth. Additionally, X-ray diffraction (XRD) was employed to identify the phase information of Zn foils after cycling. As Fig. 2h shows, after cycling in the ZSO+5PPS electrolyte, the intensity ratio of characteristic peaks corresponding to Zn (002) and (100) crystal planes is elevated to 1.84, while it is only 1.30 after cycling in the pristine electrolyte, implying that the Zn deposition in the PPS-added electrolyte is more compact and flatter [68].

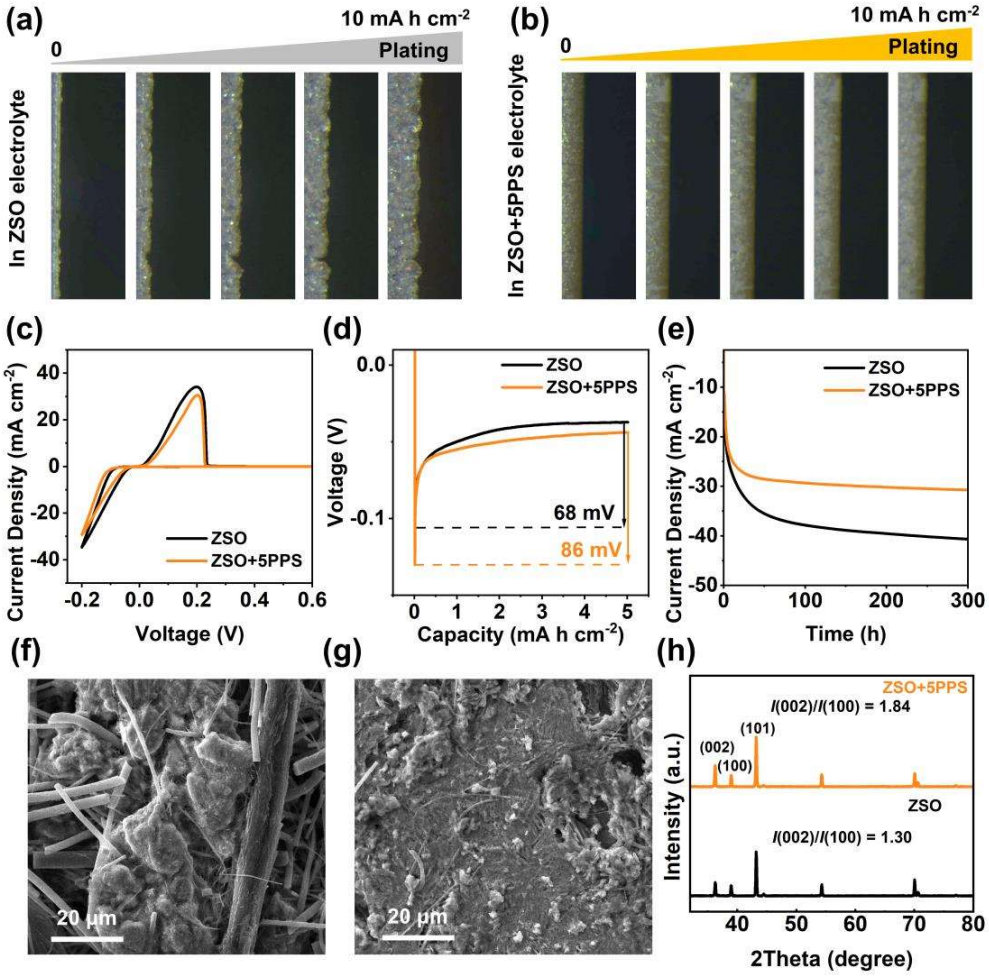

Fig. 2. *In-situ* OM observation of Zn electrodeposition process at 10 mA cm^{-2} for 1 h

in (a) ZSO electrolyte and (b) ZSO+5PPS electrolyte, respectively; (c) the first cycle of CV curves of Zn//Cu asymmetric batteries using ZSO and ZSO+5PPS electrolytes; (d) initial nucleation overpotential of Zn//Cu asymmetric batteries assembled with different electrolytes; (e) CA curves of Zn//Zn symmetric batteries assembled using ZSO and ZSO+5PPS electrolytes under a constant overpotential of −150 mV; SEM images of Zn electrode surface after 20 cycles in (f) ZSO electrolyte and (g) ZSO+5PPS electrolyte at 10 mA cm^{-2} and 10 mA h cm^{-2}; and (h) corresponding XRD patterns.

2.4 Study on the inhibition of side reactions by PPS additives

To confirm and better understand the beneficial roles of PPS additive in the inhibition of side reactions, a series of electrochemical measurements and material characterizations were carried out. Linear polarization (LP) tests were adopted to quantify the corrosion rate of Zn electrodes in ZSO electrolytes without and with PPS. As shown in Fig. 3a, the corrosion current density (j_{corr}) acquired from Tafel plots is drastically reduced from 5.81 to 3.52 mA cm^{-2} when 5 mM PPS was added to the ZSO electrolyte, which confirms the suppression of undesirable Zn corrosion in aqueous electrolytes. LSV measurements were also performed to verify the inhibition of HER by PPS. To exclude the interference from Zn deposition, 0.5 M Na_2SO_4 (denoted as NSO) electrolytes without and with 5 mM PPS were used to replace ZSO in LSV test. Fig. 3b shows that the electrolyte with PPS exhibits a significantly reduced current response of HER compared to the blank electrolyte, demonstrating the effectiveness of PPS additive in hindering water decomposition, which is probably due to the lean-water

EEI constructed by the adsorbed PPS molecules [36]. To further explore the protective capability of PPS, EIS tests were conducted on Zn//Zn symmetric batteries with ZSO and ZSO+5PPS electrolytes after resting for 24 h. Nyquist plots in Fig. 3c reveal that the PPS-containing electrolyte leads to a smaller R_{ct} of the symmetric battery after resting, which can be ascribed to the suppressed formation of passivation products [37]. Furthermore, the protection effect of PPS on Zn against side reactions was also studied by immersing Zn electrodes in both ZSO and ZSO+5PPS electrolytes for 7 days. SEM image (Fig. 3d) shows that a large number of passivation product flakes appear on the surface of Zn foil immersed in PPS-free electrolyte. On the contrary, the surface of Zn foil soaked in PPS-containing electrolyte maintains a flat morphology (Fig. 3e), which is similar to that of the pristine Zn foil shown in Fig. S12. XRD patterns in Fig. 3f verify that passivation products of Zn foil immersed in ZSO electrolyte feature much stronger intensity than those in the ZSO+5PPS electrolyte. The side reaction suppression capability of ZSO+5PPS electrolyte was further proved using the "reservoir half-cell" method [30, 57]. Specifically, Zn//Cu asymmetric batteries were first cycled with 2 plating/stripping cycles with a current density of 2 mA cm^{-2} for 0.5 h and a charge cut-off voltage of 0.5 V to eliminate the potential interference of irrelevant factors, including the formation of CuZn alloy and surface roughness of Cu foil current collectors [17, 48]. After that, 1 mA h cm^{-2} (Q_p) of Zn, which was used as a "reservoir", was electroplated onto the Cu counter electrode at a current density of 2 mA cm^{-2}. Zn//Cu batteries were subsequently cycled at a fixed areal capacity of 0.4 mA h cm^{-2} (Q_c) 20 times, followed by stripping to a cut-off voltage of 0.5 V to remove all of the

Zn (Q_s) on the surface of Cu foil. The CE can therefore be calculated by the following equation:

$$CE = (20Q_c + Q_s)/ (20Q_c + Q_p)$$

Fig. 3g and h show that the Zn//Cu cell with the ZSO+5PPS electrolyte exhibits a higher CE (97.61%) than that without PPS (97.18%), confirming that the PPS additive can effectively suppress side reactions and improve the reversibility of Zn plating/stripping. Furthermore, CV tests were also performed to assess the reversibility of Zn//Cu asymmetric batteries with different electrolytes. CV profiles and corresponding chronocoulometry curves in Fig. S16 further proves that the asymmetric cell with ZSO+5PPS electrolyte exhibits higher CEs than that assembled with ZSO electrolyte.

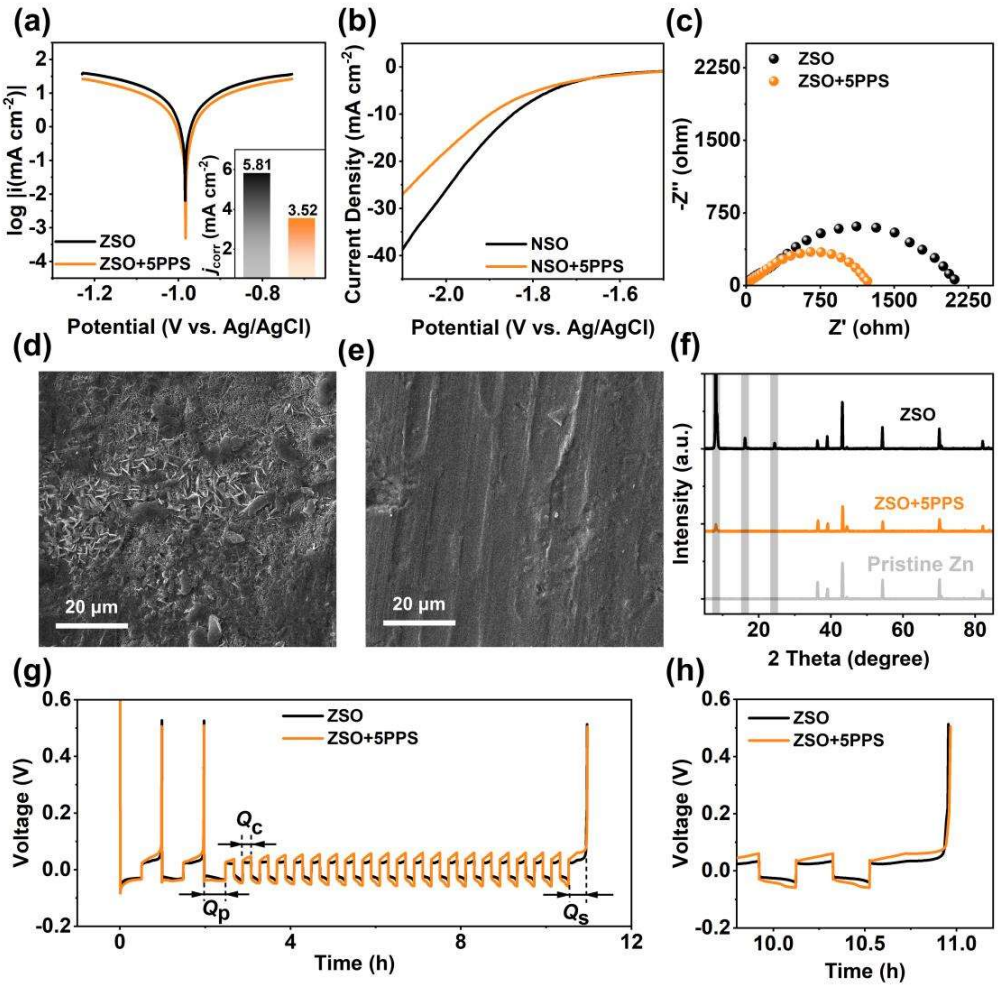

Fig. 3. (a) Tafel plots of Zn anodes measured in ZSO and ZSO+5PPS electrolytes, with inset showing the corresponding corrosion current densities; (b) LSV curves for HER in NSO electrolytes with and without PPS additive; (c) Nyquist plots derived from EIS tests of Zn//Zn symmetric batteries using ZSO and ZSO+5PPS after resting for 24 h; surface morphology observed by SEM of Zn foils soaked for 7 days in (d) ZSO and (e) ZSO+5PPS electrolytes; (f) XRD patterns of pristine Zn foil and Zn foils soaked in different electrolytes for 7 days; (g) CE tests of Zn//Cu asymmetric batteries with different electrolytes with "reservoir half-cell" method; and (h) comparison of fully stripping voltage profiles of Zn on Cu in different electrolytes.

2.5 Electrochemical performance of Zn//Zn symmetric batteries and Zn//Cu asymmetric batteries

Long-term stability is a vital metric for evaluating the practicality of Zn anodes. To this end, long-term GCD tests were carried out using Zn//Zn symmetric cells with ZSO electrolyte and ZSO+5PPS electrolyte. As illustrated in Fig. 4a, the cell using ZSO electrolyte suffers from short-circuit after only ~120 h at a current density of 2 mA cm^{-2} and an areal capacity of 1 mA h cm^{-2}. In contrast, the addition of PPS considerably extends the lifespan to more than 3,000 h. The significantly extended cycle life is attributed to the PPS-regulated EEI that effectively inhibits the formation of Zn dendrites and alleviates side reactions, which is further evidenced by the negligible increase in polarization of the symmetric battery with the ZSO+5PPS electrolyte after 3,000 cycles. More remarkably, even under harsh test conditions (1 mA cm^{-2}, 10 mA h cm^{-2} and 2 mA cm^{-2}, 20 mA h cm^{-2}), Zn//Zn symmetric batteries using PPS-added electrolyte achieve lifespans over 220 and 200 h, in sharp contrast to 60 and 17 h for Zn//Zn batteries with conventional electrolyte (Fig. S17). In addition, the Zn//Zn symmetric battery using the ZSO+5PPS electrolyte can maintain stable operation for over 400 h at 20 mA cm^{-2} and 20 mA h cm^{-2} with a cumulative plating capacity (CPC) of over 4 A h cm^{-2}, whereas the battery using ZSO electrolyte fails after only 35 h (Fig. 4b). Moreover, to fulfill the practical application requirements, RAZBs should be operated stably at high DoD with a limited supply of Zn [69]. Therefore, thinner Zn foils (50 μm) were used as electrodes in symmetric batteries. These batteries were tested

at a high current density of 20 mA cm^{-2} with a DoD of up to 70%. As can be seen in Fig. 4c, the PPS-modified electrolyte allows the Zn//Zn symmetric battery to charge and discharge for more than 250 h, whereas the battery without PPS additive failed in less than 80 h. In addition, the rate capability of Zn//Zn batteries with two different electrolytes was assessed. With a fixed areal capacity of 1 mA h cm^{-2}, Zn//Zn symmetric batteries were first tested at a gradually increased current density of 0.5, 1, 5, 10, 20, and 30 mA cm^{-2}, followed by GCD test at 1 mA cm^{-2}. As shown in Fig. 4d**,** both Zn//Zn batteries using ZSO electrolyte and ZSO+5PPS electrolyte can normally operate during the stage of increasing current density. However, the battery with pure ZSO electrolyte suffers from abrupt failure in the following GCD test, which is primarily attributed to the uneven electrode surface and accumulated side reaction products formed during the prior plating/stripping cycles. In stark contrast, the ZSO+5PPS electrolyte allows the Zn//Zn symmetric battery to stably cycle when returned to a small current density, demonstrating the superior rate capability. Furthermore, it is shown in Fig. 4e that CPC provided by Zn batteries in this work outperforms most recently reported high-performance Zn//Zn symmetric batteries achieved by electrolyte additives, highlighting the superiority of the ZSO+5PPS electrolyte designed in this work. Fig. 4f displays the CEs of Zn//Cu asymmetric batteries over long-term cycling. It is found that the introduction of PPS additive enables Zn//Cu asymmetric batteries to achieve an ultra-high CE of up to 99.88% and an ultralong cycle life of more than 4,000 cycles (about half a year), confirming suppressed side reactions and dendrite formation of Zn anode in the presence of PPS. By contrast, the asymmetric battery using a pristine electrolyte

shows a relatively lower CE of 99.65% and can only sustain 210 cycles due to the severe side reactions and dendrite formation (Fig. S18). Fig. 4g further reveals that voltage-capacity curves of the asymmetric cell using ZSO+5PPS electrolyte are very smooth and almost coincide with each other after different cycles, demonstrating the outstanding stability and reversibility of Zn anodes enabled by PPS modulation. More impressively, both CEs and lifespan of asymmetric cells achieved in this work surpass those reported in relative works (Table S1), further demonstrating the superiority of PPS electrolyte additive.

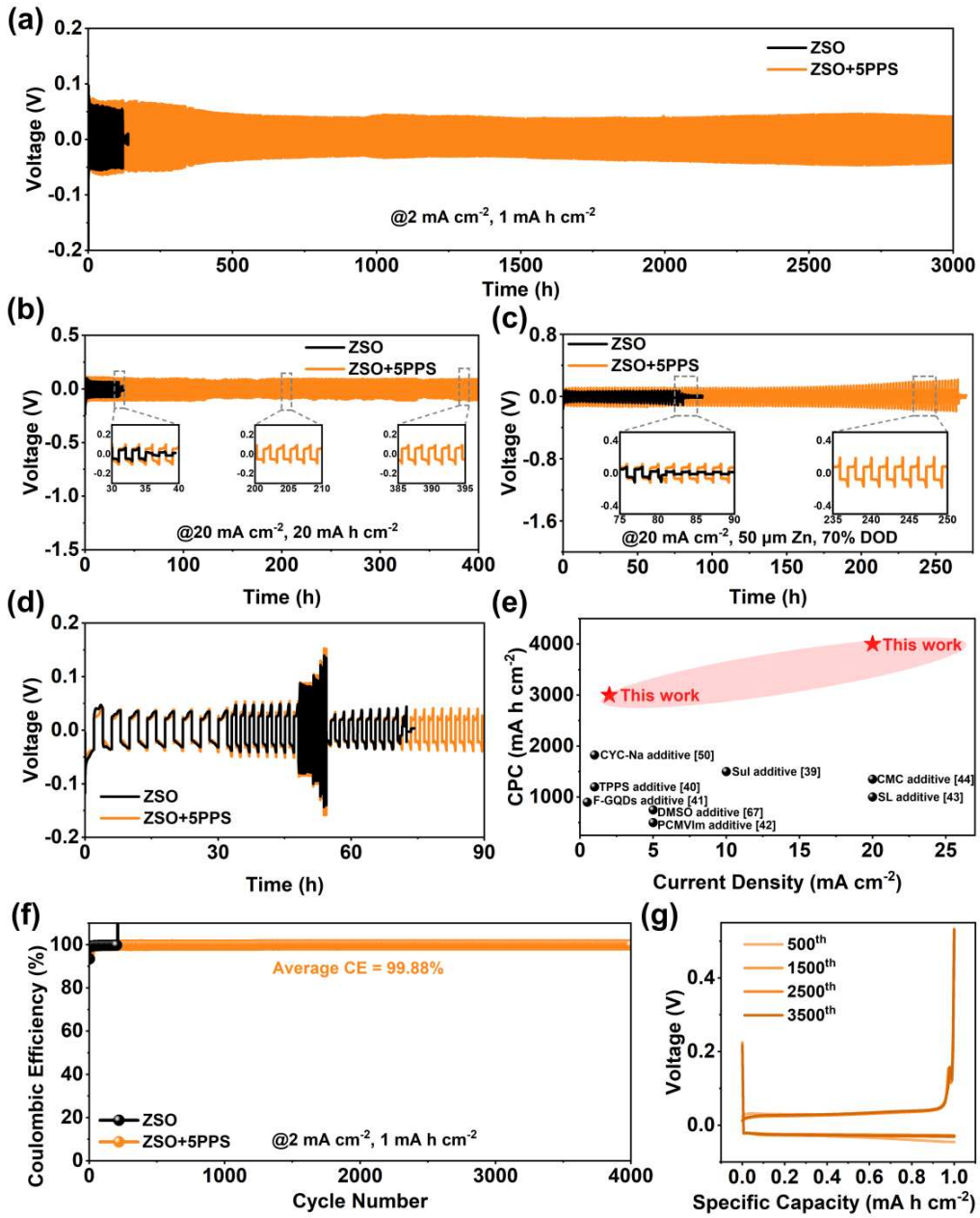

Fig. 4. Long-term GCD tests of Zn//Zn symmetric batteries using ZSO and ZSO+5PPS electrolytes at (a) 2 mA cm^{-2} with an areal capacity of 1 mA h cm^{-2}, (b) 20 mA cm^{-2} with an areal capacity of 20 mA h cm^{-2}, and (c) 20 mA cm^{-2} and 70% DoD with 50-μm-thick Zn foils; (d) rate capability of Zn//Zn symmetric batteries assembled with ZSO and ZSO+5PPS electrolytes; (e) comparison of the CPC of Zn//Zn symmetric batteries using ZSO+5PPS electrolyte with recently reported related works; (f) CEs of

Zn//Cu asymmetric batteries using ZSO and ZSO+5PPS electrolytes at 2 mA cm^{-2} with an areal capacity of 1 mA h cm^{-2}; and (g) Zn plating/stripping curves of Zn//Cu battery with ZSO+5PPS electrolyte after certain cycles.

Drawing on the above studies, the detailed working mechanism of PPS additive was proposed and illustrated in Fig. 5. As can be seen, EEI in the conventional electrolyte is filled with water molecules in addition to the solvated Zn^{2+}. As a result, the Zn anode suffers from severe side reactions caused by water decomposition and rampant dendrite growth resulting from random diffusion and deposition of Zn^{2+}, leading to the poor reversibility and thus short cycle life of RAZBs. In contrast, in the designed electrolyte, PPS will be preferentially adsorbed on Zn anode surface, effectively repelling water molecules and thus forming a water-poor EEI, which considerably alleviates the interfacial side reactions. Meanwhile, adsorbed PPS additives play a pivotal role in facilitating homogeneous diffusion and nucleation of Zn^{2+}, thereby suppressing the formation and growth of Zn dendrites. Consequently, the cycle life of RAZBs with ZSO+5PPS electrolytes is significantly extended. More importantly, it should be noted that PPS is non-consumable, which enables it to dynamically regulate a conducive EEI for the reversible operation of Zn anodes, even under high DoD and limited Zn supply.

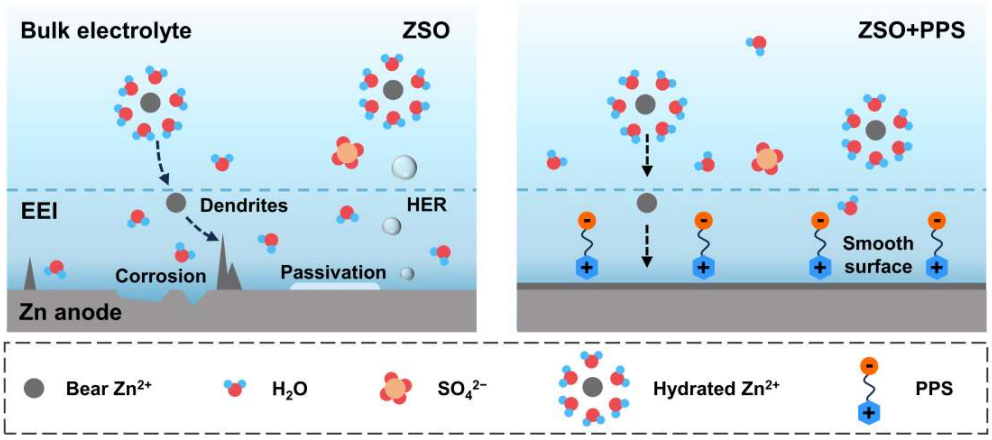

Fig. 5. Schematic illustrations of Zn deposition in ZSO and ZSO+5PPS electrolytes.

2.6 Electrochemical performance of full batteries and hybrid supercapacitors

To further verify the applicability of PPS-modulated electrolyte, various cathode materials (α-MnO_2, $Cu_xV_2O_5{\cdot}nH_2O$, $NaV_3O_8{\cdot}1.5H_2O$ (NVO), and AC) were coupled with Zn electrodes to prepare full batteries and hybrid supercapacitors. α-MnO_2 nanorods (based on XRD pattern and SEM images, Figs. S20 and S22) were synthesized by a simple hydrothermal method [49]. For Zn//α-MnO_2 full batteries, 0.1 M $MnSO_4$ was added to both ZSO and ZSO+5PPS electrolytes to inhibit the dissolution of the MnO_2 cathode [70]. The CV curves of Zn//α-MnO_2 batteries with different electrolytes are shown in Fig. S23. Two pairs of similarly shaped redox peaks confirm that PPS does not undergo a reaction in Zn//α-MnO_2 full batteries. The rate capability of full batteries was then tested by gradually raising current densities from 1 to 5 A g^{-1}, followed by reducing back to 1 A g^{-1}. As displayed in Figs. 6a, 6b, and S24, the designed electrolyte enables the full battery to deliver an average specific capacity of 252, 184, 146, 122, and 105 mA h g^{-1} at the current densities of 1, 2, 3, 4, and 5 A g^{-1},